High-resolution imaging of surface acoustic wave scattering

T. Hesjedal[a)]
Solid State and Photonics Lab, CIS-X, Stanford University, Stanford, California 94305-4075

G. Behme
Paul Drude Institute for Solid State Electronics, Hausvogteiplatz 5–7, D-10117 Berlin, Germany

(Received 20 November 2000; accepted for publication 29 January 2001)

We examine the scattering of surface acoustic waves (SAWs) by single dots, periodic and locally damped two-dimensional dot lattices. Employing the scanning acoustic force microscope, SAW fields are imaged with nanometer resolution. We study the influence of a roughly wavelength-sized single dot on SAW diffraction. In order to distinguish between forward- and backscattered components, we insonify the dot with the pump and probe beam under 0° and 90°. We furthermore analyze the SAW diffraction by a regular dot array. The wave field appears to be localized around the dots. Adding surface distortions, the regular SAW localization pattern brakes down in the vicinity of the distortion. © *2001 American Institute of Physics.* [DOI: 10.1063/1.1357453]

The spatially resolved investigation of surface acoustic wave (SAW) scattering is of great fundamental as well as technological interest. A large variety of SAW scattering structures have been fabricated and investigated in detail.[1] The structures are usually periodic ensembles of elastic inhomogeneities, such as metal or dielectric films or etched grooves or pits. Any given structure can be conveniently subdivided into stripes and dots. A dot, which is the focus of this work, is defined as any elastic inhomogeneity with dimensions of at most a few wavelengths in any direction. The importance of the dot array for acoustic devices comes from the fact that it exhibits a designable frequency transfer function and thus additional ways to manipulate SAW propagation. Examples of reflective dot array devices in the past are SAW pulse-compression filters[2] or multichannel filters.

There has also been a growing interest in the study of two-dimensional (2D), periodic, elastic structures known as phononic crystals.[3] First, they serve as easy-to-fabricate model systems for electronic or photonic localization studies. Photonic crystals, for instance, are in high demand because they offer enormous opportunities for manipulating light in new ways. Second, phononic crystals offer the possibility to create acoustic phonon band gaps manipulating the electron-phonon interaction. Furthermore, phononic crystals are of interest as functional elements of SAW devices. Measurements and calculations of SAW localization have been reported in one-dimensional Fibonacci superlattices,[4] as well as in 2D periodic elastic structures.[5,6]

The most common tool for *local* probing of SAW scattering[7] and localization[8] experiments are laser-optical methods. Using noncontacting optical excitation and detection schemes, the acoustic wave dispersion of phononic crystals can be mapped out conveniently.[9] However, due to their diffraction limited lateral resolution, the detailed investigation of technologically interesting future devices in the gigahertz range, i.e., submicron wavelengths, is somewhat limited. In this letter, we focus on the spatially resolved investigation of SAW scattering by single dots, as well as regular and locally damped dot arrays by scanning acoustic force microscopy (SAFM).

The SAFM[10,11] is a tool for the nanoscale investigation of arbitrarily polarized SAW fields[12] (see Fig. 1). It is based on conventional force microscopy and capable of detecting the phase and amplitude of SAWs in the megahertz to gigahertz frequency range. It has been used, e.g., to characterize SAW devices with high lateral resolution.[13]

In the standard SAFM setup, two high-frequency (rf) SAWs which are excited by interdigital transducers (IDTs) insonify the region of interest. Due to the nonlinearity of the force-distance curve, the acoustic waves are mixed at the mechanical tip-sample contact.[14] By choosing the excitation frequencies to be slightly different, contributions at multiples of the difference frequency and also higher harmonics of the rfs are expected. However, as the detection bandwidth of the cantilever is roughly given by its resonance frequency (of typically some 10 kHz), only the signal at the difference frequency is detected delivering the phase and amplitude of the SAW. The mechanical detection system thus resembles a diode followed by a low-pass filter.

The phase signal that can be expected in an ideal collinear SAW propagation experiment is a linear function of propagation distance.[14] Hereby, the slope is given by the k vectors only, and can, in return, be used to measure the phase velocity locally. Within the propagating SAW beams, the ideal amplitude response is constant. In a noncollinear SAW experiment (Fig. 1), the phase still exhibits a linear signal response, however, the signal plane is rotated with respect to

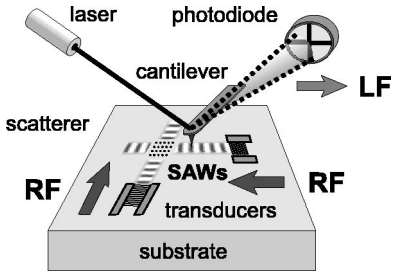

FIG. 1. Schematic representation of the SAFM.

a)Electronic mail: thorsten@snow.stanford.edu

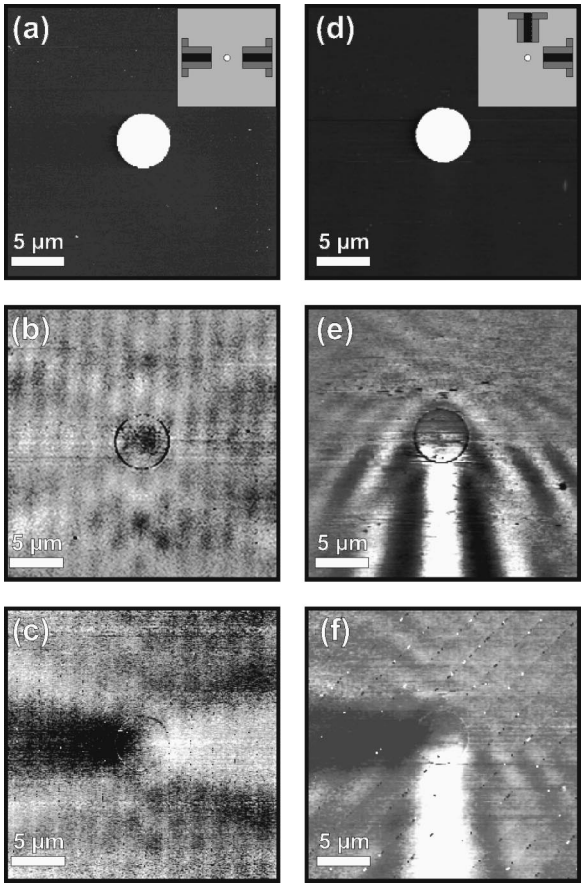

FIG. 2. SAFM topography (a), (d), amplitude (b), (e), and phase deviation images (c), (f) of a scattering dot (Au, diameter 5 μm) on (001) GaAs for 0° (a)–(c) and 90° (d)–(f) sampling geometries. The SAWs were launched along [100] directions (+5 dBm, from the bottom or left and −5 dBm, from the right) with $\lambda_{SAW}=3.3\ \mu$m.

the propagation vectors. The rotation angle, conversely, allows for the measurement of both k vectors simultaneously.[15] The expected amplitude signal is again constant.

Scattered wave components, on the other hand, lead to deviations of this simple picture and can consequently easily be identified. Moreover, SAW mixing experiments allow the detection of extremely small oscillation components since signals with amplitude differences of 40 dB can still be detected.[16]

For the investigation of wave scattering from a single dot, a collinear and a perpendicular wave propagation geometry was realized in order to distinguish between forward- and backscattered wave components. The circular scattering object (Au, diameter: 5 μm, thickness: 50 nm) on (001) GaAs was insonified in [110] directions, i.e., equivalent Rayleigh waves can be launched in perpendicular directions, at a frequency of 860 MHz ($\lambda=3.3\ \mu$m). The topography is shown in Figs. 2(a) and 2(d).

In the collinear geometry [Figs. 2(a)–2(c)], forward- and backscattered components are superimposed to the incident waves. The SAFM amplitude image [Fig. 2(b)] exhibits a point-symmetric pattern and, additionally, an underlying standing wavefield. The standing wavefield is induced by SAW reflections at the respective opposing transducers. It becomes visible in the amplitude and the phase images through the additional contribution to the Δf cantilever oscillation with an exactly inverted phase term. Moreover, wave field patterns that have to be attributed to the influence of the scatterer are visible. A roughly circular amplitude pattern surrounds the object. In the incident SAW propagation direction an amplitude maximum is found. Additionally, a higher amplitude is obtained following directions 30° off the incident waves.

The phase image (not shown) follows a perfectly linear pattern, with slight deformations at the position of the Au dot. This is due to the different SAW phase velocities of Au and GaAs (which can also be locally measured this way). The linear contribution to the contrast was subtracted from the phase image in order to obtain the contrast that is related to the scattered components, i.e., waves that do not contribute to the primary wave's mixing signal. The phase deviation image [Fig. 2(c)] obtained this way shows an antisymmetric pattern with phase lags of alternate sign for both propagation directions. The positions of the lock-in related 360° phase jumps remain visible as artifacts (dots) in the phase deviation images.

In the noncollinear geometry [Figs. 2(d)–2(f)], the Rayleigh waves are launched by two perpendicular transducers (see inset). The top IDT was fed with an input power that was 10 dB higher than for the IDT on the right. Thus, the wave field generated by this transducer dominates the SAFM amplitude contrast. In the wave shadow of the dot, an area of very high amplitude is found, surrounded by regions of very low amplitude. Backreflected waves form additional smaller maxima in front of the dot, similar to a ship's bow wave. The amplitude image thus resembles a pole in streaming water.

The phase image (not shown) again exhibits a linear behavior that was subtracted to obtain the phase deviation image. However, the phase fronts are rotated by 45° as perpendicular, but otherwise identical waves were mixed. First, the phase deviation image [Fig. 2(f)] again reveals a slope at the position of the dot reflecting the different elastic materials properties. Around the dot, the scattered components dominate the phase deviation image. However, in contrary to the amplitude image, the waves scattered along both propagation directions are influenced equally by the dot exhibiting a phase lag. Due to the SAFM mixing, the phase delay has a different sign for the two directions; it is positive (bright area) for the vertical, and negative (dark area) for the horizontal direction.

The face-centered-cubic dot lattice (lattice spacing: $\Delta x=4\ \mu$m, width: 100 μm) consisted of Au dots (diameter: 1 μm, thickness: 45 nm). It was fabricated in the center of two crossed delay lines on (001) GaAs where Rayleigh waves can be launched in perpendicular [110] directions at a frequency of 694 MHz ($\lambda=4.0\ \mu$m, acoustic aperture: 65 μm) towards it. Figure 3(a) shows a 20 μm scan close to the edge of the regular dot lattice. Two collinear IDTs of the device (right and left of the array) were powered with 5 dBm. The phase image (b) shows to the first order a linear phase behavior, which appears as a saw-tooth shaped structure due to the 360° limit of the lock-in. At the positions of the dots, the phase fronts are strongly deformed. Between two dots along the phase front, the phase again shows the pure linear behavior. However, towards the dots a phase lag becomes obvious indicating scattered components. In the corresponding ampli-

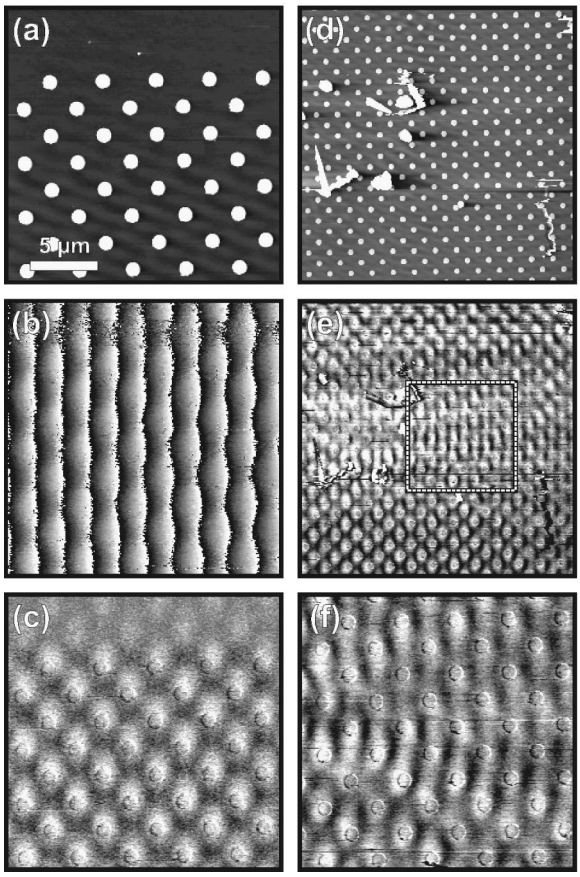

FIG. 3. Topographies (a), (d), phase (b), and amplitude (c), (e), (f) SAFM scans of a 2D scattering dot array (Au, $d=1\ \mu$m; fcc, $\Delta x=4\ \mu$m; $\lambda_{SAW}=4.0\ \mu$m). Images (a)–(c) show the results for the periodic array, and (d)–(f) the results for the locally damped array.

tude image (c), we find regular, localized spots of high wave amplitude at the dot positions. Outside the dot lattice (at the upper edge of the image), the signal quickly decays. It has to be noted that the SAFM amplitude image is not a snapshot of the surface movement but the envelope at the high frequency.

Finally, we investigated a locally damped dot lattice. The distortions were weakly coupling surface contaminations that mainly lead to a local wave amplitude damping. Figure 3(d) displays a 50 μm topography scan. The corresponding amplitude image (e) shows the same apparent amplitude localization as in (c) above and below the locally damped region. The amplitude appears to be concentrated in certain angular regions around the defects. The 20 μm zoom (f) of the amplitude [the inset in (e) indicates the relative position] confirms the wave reflection preferably under an angle of 25° with respect to the horizontal propagation direction (measured from the localized distortion).

In this letter, we have demonstrated that the SAFM is a useful method for the local investigation of scattering phenomena of a single dot, as well as dot arrays. We found that the wave amplitude is localized around the dots and that local surface defects strongly affect the amplitude pattern. In the future, SAFM will be used for detailed SAW localization studies and it may be used for local SAW absorption studies by quantum dots,[17] too.

This work was supported by the DFG and made use of the Stanford Nanofabrication Facility funded by the National Science Foundation under Award No. ECS-9731294.

[1] L. P. Solie, Appl. Phys. Lett. **28**, 420 (1976).
[2] H. van de Vaart and L. P. Solie, Appl. Phys. Lett. **31**, 1 (1977).
[3] M. S. Kushwaha, P. Halevi, L. Dobrzynski, and B. Djafarirouhani, Phys. Rev. Lett. **71**, 2022 (1993).
[4] L. Macon, J. P. Desideri, and D. Sornette, Phys. Rev. B **44**, 6755 (1991).
[5] Y. Tanaka and S. Tamura, Phys. Rev. B **58**, 7958 (1998).
[6] R. E. Vines and J. P. Wolfe, Physica B **263–264**, 567 (1999).
[7] S. Tuli, A. B. Bhattacharyya, and D. Fournier, Appl. Phys. Lett. **67**, 1844 (1995).
[8] L. Dhar and J. A. Rogers, Appl. Phys. Lett. **77**, 1402 (2000).
[9] J. A. Rogers, A. A. Maznev, M. J. Banet, and K. A. Nelson, Annu. Rev. Mater. Sci. **30**, 117 (2000).
[10] W. Rohrbeck and E. Chilla, Phys. Status Solidi A **131**, 69 (1992).
[11] T. Hesjedal, E. Chilla, and H.-J. Fröhlich, Appl. Phys. A: Mater. Sci. Process. **61**, 237 (1995).
[12] G. Behme, T. Hesjedal, E. Chilla, and H.-J. Fröhlich, Appl. Phys. Lett. **73**, 882 (1998).
[13] T. Hesjedal, E. Chilla, and H.-J. Fröhlich, Appl. Phys. Lett. **70**, 1372 (1997).
[14] E. Chilla, T. Hesjedal, and H.-J. Fröhlich, Phys. Rev. B **55**, 15852 (1997).
[15] G. Behme and T. Hesjedal, Appl. Phys. Lett. **77**, 759 (2000).
[16] T. Hesjedal and G. Behme, Electron. Lett. **36**, 1903 (2000).
[17] G. R. Nash, S. J. Bending, M. Boero, M. Riek, and K. Eberl, Phys. Rev. B **59**, 7649 (1999).